frontiers | Frontiers in Environmental Science

TYPE Original Research
PUBLISHED 16 October 2024
DOI 10.3389/fenvs.2024.1485328

OPEN ACCESS

EDITED BY
Nsikak U. Benson,
Topfaith University, Nigeria

REVIEWED BY
Jun Wu,
Hohai University, China
Hao Zheng,
Ocean University of China, China

*CORRESPONDENCE
Lin Wang,
LinW629@163.com

RECEIVED 23 August 2024
ACCEPTED 30 September 2024
PUBLISHED 16 October 2024

CITATION
Li F, Yan Q, Li Z, Tan Z, Li Y, Wang S, Guo J, Peng H and Wang L (2024) Sorption/desorption of phenanthrene and ofloxacin by microbial-derived organic matter-mineral composites. *Front. Environ. Sci.* 12:1485328. doi: 10.3389/fenvs.2024.1485328

Sorption/desorption of phenanthrene and ofloxacin by microbial-derived organic matter-mineral composites

Fangfang Li[1], Qiuling Yan[1], Zhongwen Li[1], Zhicheng Tan[1], Yuxuan Li[1], Siyao Wang[1], Jiawen Guo[2], Hongbo Peng[1,3] and Lin Wang[1,4]*

[1]Yunnan Key Laboratory of Soil Carbon Sequestration and Pollution Control, Faculty of Environmental Science and Engineering, Kunming University of Science and Technology, Kunming, China, [2]Yunnan Sugarcane Research Institute, Yunnan Academy of Agricultural Sciences, Kaiyuan, China, [3]Faculty of Modern Agricultural Engineering, Kunming University of Science & Technology, Kunming, Yunnan, China, [4]Institute of Agricultural Resources and Environment, Sichuan Academy of Agricultural Sciences, Chengdu, China

Introduction: Soil organic matter plays an important role in the long-term "locking" of organic contaminants in soil environment. Recently, microbial-derived organic matter have been recognized as essential components of stabilized soil carbon pools. However, the contribution of microbial-derived organic matter to sorption of organic contaminants remains unclear.

Methods: Here, we obtained microbial-derived organic matter-mineral composites by inoculating model soil (a mixture of hematite and quartz sand (FQ) or montmorillonite and quartz sand (MQ)) with natural soil microorganisms and different substrate-carbon (glycine (G), glucose (P), or 2, 6-Dimethoxyphenol (B)), which were named GF, PF, BF, GM, BM, and PM, respectively. Batch sorption/desorption experiments were conducted for phenanthrene (PHE) and ofloxacin (OFL) on the composites.

Results and Discussion: The composites cultured with 2,6-dimethoxyphenol had the highest carbon content (0.98% on FQ and 2.11% on MQ) of the three carbon substrates. The carbon content of the composites incubated with MQ (0.64%–2.11%) was higher than that with FQ (0.24%–0.98%), indicating that montmorillonite facilitated the accumulation of microbial-derived organic matter owing to its large specific surface area. The sorption of PHE by microbial-derived organic matter was mainly dominated by hydrophobic partitioning and π-π conjugation, whereas the sorption of OFL was mainly dominated by hydrophobic hydrogen bonding and π-π conjugation. The sorption of OFL onto the composites was more stable than that of PHE. Microbial-derived organic matter -mineral composites can reduce the risk of organic contaminant migration in soil, particularly ionic organic contaminants.

KEYWORDS

microbial-derived organic matter, mineral, phenanthrene, ofloxacin, sorption, desorption

1 Introduction

The sorption of organic contaminants to soil organic matter (SOM) is a key process for controlling their transport in the environment. The traditional conceptual model of SOM considers plant-derived OM as the major contributor to SOM; thus, previous studies on the interaction of organic contaminants with SOM have been centered more on biochar (Wu et al., 2012; Ahmed et al., 2018; Chu et al., 2019; Safari et al., 2019; Xing et al., 2023) and plant-derived humus fractions (Pan et al., 2005; Wen et al., 2007; Gao et al., 2014; Su et al., 2024; Xia et al., 2024). However, our understanding of the mechanisms underlying SOM formation and stabilization has been substantially revised in recent years. With the introduction of the concept system regarding the "soil microbial carbon pump," the contribution of microbial-derived OM to soil stable carbon pool has been widely recognized, especially the contribution of microbial-derived OM (Kallenbach et al., 2016; Zhu et al., 2020; Liang and Zhu, 2021). Microbial necromasses and some metabolites are relatively stable in the soil and contribute to the soil carbon pool as microbial-derived OM (Liang et al., 2019; Buckeridge et al., 2020; Liang et al., 2020), which are produced and gradually accumulated in the soil as the microbial community grows, reproduces, and dies in an iterative process (Liang and Zhu, 2021; Hu et al., 2023). Mineral protection is essential for the stabilization of microbial-derived OM in the soil (Xiao et al., 2023). Soil minerals can form stable organic-inorganic composites with microbial-derived OM through sorption (Kaiser and Zech, 1997; Mikutta et al., 2007), sequestering (Duchaufour, 1976; Chi et al., 2019), and aggregation (Angers and Giroux, 1996) and soil mineral properties, such as type and composition affect their stability (Cai et al., 2021). Clay minerals and iron oxides can interact with pollutants through various sorption mechanisms, playing a vital role in soil environment by acting as a natural scavenger of pollutants (Abollino et al., 2003; He et al., 2015). The sorption and desorption of pollutants on clay minerals and iron oxides are important for understanding the fate of the pollutants in soil (Zhang et al., 2017). As an important source of stable carbon pools in soil, microbial-derived OM-mineral composites could closely affect the migration and transformation of organic contaminants. Recent studies reported that the microbial extracellular polymeric substances (EPS) had been shown to be effective in sorption heavy metals and organic contaminants in water (Disi et al., 2023; Yang et al., 2023; Xu et al., 2020). EPS under anaerobic conditions had a higher aromatic structure and stronger sorption capacity for pyrene (Lee et al., 2013). Furthermore, the EPS-minerals composites promoted the sorption of PHE compared to pristine EPS (Chen et al., 2020). However, current research on the interaction between microbial-derived OM-mineral composites and organic contaminants in soil is limited and the effects of the types of soil minerals and substrate-carbon (substrate-C) of the composites on the sorption of organic contaminants remain unclear.

The improper utilization of pesticides and antibiotics in human-related production activities has resulted in several unintended consequences; significant quantities of polycyclic aromatic hydrocarbons (PAHs) and antibiotics have been identified in the soil. Phenanthrene (PHE) is a representative PAH that is commonly used in various studies. It is a planar, apolar, hydrophobic, and low-molecular-weight compound that comprises three fused benzene rings and has significant carcinogenic and mutagenic toxicity to organisms (Goldman et al., 2001; Pakova et al., 2006; Shen et al., 2019; Wang et al., 2019). Ofloxacin (OFL) is a fluoroquinolone antibiotic. The presence of excess antibiotics in the environment has the potential to lead to the development of antibiotic-resistant bacteria and genes that could ultimately threaten the stability of ecosystems and human health (Zhang et al., 2015; Das et al., 2024; Na et al., 2024). It is a hydrophilic ionic compound comprised of a carboxylic acid group (pKa = 6.10) and a piperazine group (pKa = 8.28). In aqueous solution, it exists as a cation (OFL^+), an amphoteric ion ($OFL^\pm$), or an anion (OFL^-) at different pH conditions (Feng et al., 2015; Li et al., 2019). PHE and OFL were used in this study because of their environmental importance, chemical properties, and structures, which may result in different sorption and desorption behaviors.

A more systematic understanding of the interaction mechanisms between microbial-derived OM and organic contaminants in soil is required. To prepare microbial-derived OM-mineral composites, three substrate-Cs (Glycine, Glucose, or 2, 6-Dimethoxyphenol, the first two of which represent the abundant energy sources for microbial metabolic processes in natural soils, whereas the last one can be considered plant-derived organic matter) were selected. Microbial-derived OM-mineral composites were cultured with substrate-C and two model soils containing montmorillonite or hematite. Batch sorption and desorption experiments were performed on PHE and OFL. This study aimed to analyze 1) the sorption and desorption characteristics of microbial-derived OM-mineral composites incubated with different substrate-Cs to PHE and OFL, 2) the effects of different properties of microbial-derived OM-mineral composites on their sorption, and 3) the primary sorption mechanisms and stability of microbial-derived OM-mineral composites on PHE and OFL.

2 Materials and methods

2.1 Samples and reagents

In this experiment, soil microorganisms were inoculated onto the model soil and then incubated with different substrate-Cs to obtain microbial-derived OM-mineral composites. The composites were obtained by incubation with different substrates (glycine (G), glucose (P), or 2, 6-Dimethoxyphenol (B)) and two model soils (33% hematite + 67% quartz sand (FQ) or 33% montmorillonite + 67% quartz sand (MQ), w/w) for 6 months (Kallenbach et al., 2018), abbreviated as GF, PF, BF, GM, PM, and BM, respectively. FQ and MQ without the addition of substrate-C and microbial cultures were used as blank controls. In this study, we designated the composites of FQ and MQ as microbial-derived OM -hematite and microbial-derived OM-montmorillonite composites, respectively. All samples were stored at −80°C for future use. The basic physicochemical properties of the samples are listed in Supplementary Table S1.

The properties of the eight samples were characterized using elemental analyzer (EA, Vario MICRO Cude, Elementar, Germany), specific surface area analyzer (SSA, JW-BK132F, Beijing Jingwei Gaobo Technology Co., LTD., China), Fourier transform infrared spectroscopy (FTIR, Varian 640-IR, American Varian Company,

United States), and X-ray photoelectron spectroscopy (XPS, K-Alpha, American Thermo Scientific, United States). The zeta potentials of the adsorbents after sorption equilibrium were measured using a zeta potential analyzer (Nano ZEN 3600, Malvern, United Kingdom). Analytically pure PHE and OFL were provided by *Aladdin*. The physical and chemical properties of PHE (Liang et al., 2015) and OFL (Peng et al., 2012; Liang et al., 2015) are listed in Supplementary Table S2.

2.2 Batch sorption and desorption experiments

PHE (1 mg/L) and OFL (50 mg/L) were dissolved in a background solution (0.02 M NaCl and 200 mg/L NaN_3 solution) (Pan et al., 2011; Li et al., 2017) and stored in a refrigerator at 4°C for later use. The stock solutions were diluted with background solutions to obtain eight concentration ranges of 0.2–1 mg/L (PHE) and 4–50 mg/L (OFL), respectively. To exclude the influence of free dissolved organic components on the sorption of pollutants, the composites were repeatedly washed by deionized water to ensure removal of free dissolved organic components. Two parallel experiments were performed for each concentration. The sorption and desorption equilibrium times and the appropriate solid/liquid ratios were determined by preliminary experiments to maintain the sorption rates in the range of 20%–80% as much as possible to ensure the reliability of the analysis and the background solution was set as a blank reference in all experiments. Sorption experiments were performed in 8 mL amber glass vials, shaken in a shaker (150 rpm) at 25°C ± 1°C for 7 d and then centrifuged at 2,500 rpm for 5 min. The supernatant was collected and passed through the 0.45 μm membrane (SCAA-101) to prevent the solid particle impurities in the sample clogging the instrument and the concentrations of PHE and OFL were determined.

Desorption experiments were performed immediately after sorption equilibrium was reached. Desorption was studied by replacing the supernatant of the sorption equilibrium system with a new background solution. After replacing the supernatant, desorption experiments were performed under the same conditions as the sorption experiments described above and the concentrations of PHE and OFL in the supernatant were determined at the end of the experiments.

2.3 Measurement of PHE and OFL

The concentration of PHE and OFL was determined by high performance liquid chromatograph (1,260 Infinity II, Agilent, United States) with the following chromatographic conditions: flow rate of 1 mL/min, column temperature of 30°C, and injection volume of 20 μL. The mobile phase for PHE was a mixture of methanol and ultrapure water at a ratio of 9:1 (v/v) at a detection wavelength of 250 nm. The mobile phase of the OFL was a mixture of 18% acetonitrile, 0.8% acetic acid, and 81.2% ultrapure water with a detection wavelength of 286 nm.

2.4 Data processes

For sorption and desorption isotherm analysis, the following three models were used:

Henry model:

$$Q_e = K_d \cdot C_e + m \tag{1}$$

Freundlich model:

$$lg\, Q_e = lg\, K_F + n\, lg\, C_e \tag{2}$$

Langmuir model:

$$Q_e^{-1} = Q_m^{-1} + (K_L \cdot Q_m \cdot C_e)^{-1} \tag{3}$$

where Q_e (mg/kg) is the equilibrium solid-phase concentration, and C_e (mg/L) is the aqueous phase concentration. K_d is the distribution coefficient, and is the vertical intercept. K_F is the Freundlich affinity coefficient and n is the Freundlich nonlinearity factor. Q_m (mg/kg) is the maximum amount of PHE and OFL per unit mass of adsorbent, K_L is the Langmuir coefficient.

Because of the different numbers of coefficients in Equations 1–3, the adjustable determination coefficient (r^2_{adj}) was used to compare the model fitting effect and the calculation formula is as follows (Equation 4):

$$r^2_{adj} = 1\text{-}\frac{m\text{-}b}{m\text{-}1}\, r^2 \tag{4}$$

where m is the number of data points used for fitting and b is the number of coefficients in the fitting equation.

Desorption of PHE and OFL was analyzed based on the release rate and the release rate (RR) of the adsorbed contaminants was calculated as follows (Equation 5):

$$RR = 1\text{-}\frac{Q_{e2}}{Q_{e1}} \tag{5}$$

where Q_{e1} (mg/kg) is the solid-phase concentration at the beginning of desorption and Q_{e2} (mg/kg) is the solid-phase concentration after desorption.

3 Results and discussion

3.1 Characteristics of microbial-derived OM-mineral composites

The elemental analysis and specific surface area (SSA) of the eight samples are presented in Table 1. The coverage of microbial-derived OM on a mineral surface can lead to a decrease in SSA. The SSA of FQ and MQ were larger than those of the composites, with SSA of 2.774 m^2/g and 36.363 m^2/g, respectively. The SSA of GF, PF, and BF were approximately 1 m^2/g and those of BM, GM, and PM were similar, ranging 7.649–8.856 m^2/g. The carbon contents on the montmorillonite composites (0.64%–2.11%) were higher than that on the hematite composites (0.24%–0.98%) and the C/H ratio of BM (1.10) was much higher than that of the other composites (C/H ratio values ranged from 0 to 0.42), which indicated a higher aromaticity in BM.

TABLE 1 Physicochemical properties of microbial-derived OM-mineral composites including the elemental analysis and specific surface area.

Name	Elemental analysis						SSA (m^2/g)	Pore volume cm^3/g	Pore radius nm
	N%	C%	H%	O%	C/H	(N+O)/C			
GF	0.02	0.24	0.14	4.73	0.14	14.85	1.075	0.005	19.059
PF	0.02	0.64	0.24	3.19	0.23	3.77	1.069	0.007	24.860
BF	0.01	0.98	0.35	7.08	0.24	5.43	0.953	0.006	25.259
FQ	0.01	0.04	0.06	1.14	—	—	2.774	0.012	16.306
GM	0.20	0.64	0.73	5.54	0.07	6.76	7.649	0.034	17.150
PM	0.15	1.54	0.31	5.91	0.42	2.96	8.856	0.037	16.110
BM	0.06	2.11	0.16	6.33	1.10	2.27	8.611	0.040	18.252
MQ	0.01	0.00	0.06	0.91	—	—	36.363	0.073	7.801

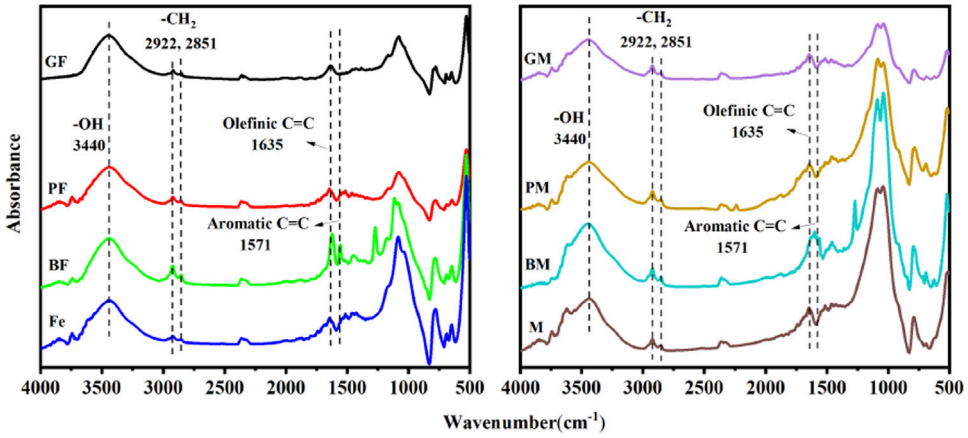

FIGURE 1
FTIR spectra of microbial-derived OM-mineral composites.

The FTIR spectra of the composites are shown in Figure 1. Peaks were observed at 3,440 cm^{-1}, which were caused by -O-H vibrations (Papageorgiou et al., 2010; Zhao et al., 2021), indicating the presence of crystalline hydrates in the eight samples. Olefinic C=C stretching vibrational peaks were observed at 1,635 cm^{-1} in eight samples (Shukla et al., 2007; Tabak et al., 2019; Feng et al., 2021), and aromatic C=C stretching vibrational absorption peaks were observed at approximately 1,571 cm^{-1} (Gauthier et al., 2005; Chen et al., 2020). In the microbial-derived OM-montmorillonite composites, BM demonstrated the highest peak intensities at 1,635 cm^{-1} and 1,571 cm^{-1}, indicating that BM contains more unsaturated carbon. The aliphatic methylene in peaks were observed at 2,922 cm^{-1} and 2,851 cm^{-1} (Mohan et al., 2016; Bolyard et al., 2019; Yan et al., 2020). The composite obtained by 2, 6-dimethoxyphenol contained more aliphatic methylene groups. The microbial-derived OM-montmorillonite composites were generally more hydrophobic than the microbial-derived OM-hematite composites.

The XPS wide-scan spectra of the microbial-derived OM-mineral composite (Supplementary Figure S1) revealed the presence of C (C1s), O (O1s), and N (N1s) on the surfaces of the eight samples at approximately 285, 532, and 400 eV, however, with different intensities. Deconvolution of C1s, O1s, and N1s spectra, respectively (Figure 2), C1s can be deconvolved into three peaks, which could be ascribed to C-C (248.8 Ev), C-O (286.46 eV), and C=O (288.57 eV) (Cheng et al., 2018; Chen et al., 2024); O1s has two peaks at 529.8 eV and 532.2 eV, which could be attributed to the O forms of Fe-O and C-O (Luo et al., 2017; Cheng et al., 2018; Chen et al., 2024; Li et al., 2024); the nuclear energy level spectrum of N1s has two peaks, which are N forms in neutral amine-NH_2 (nonprotonated) and protonated amine-NH_3, with binding energies of 399.9 eV and 402 eV, respectively (Zhu et al., 2017; Cheng et al., 2018; Olayo et al., 2023). The surface elemental compositions and assignments of the eight samples are listed in Table 2. Among the microbial-derived OM bound to hematite, PF had the highest surface carbon content (up to 20.23%), GF had the lowest (6.56%), and the surface oxygen contents of GF and FQ were lower than those of PF and BF. In the microbial-derived OM-montmorillonite composite, the highest carbon content was found on the surface of the BM (9.28%) and the surface carbon contents of GM, PM, and MQ were similar (6.03%, 5.14%, and 4.35%, respectively). In addition, the microbial-derived

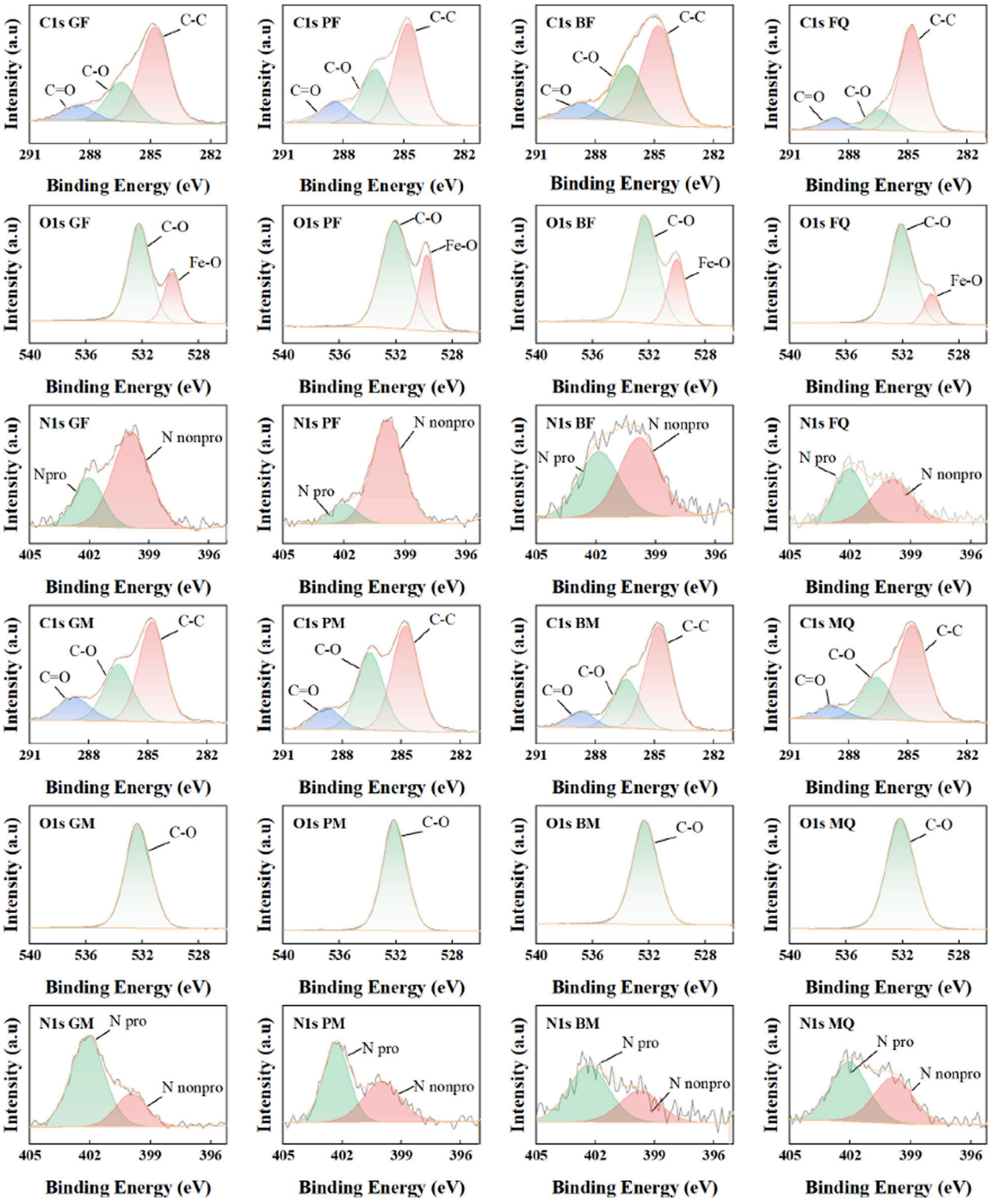

FIGURE 2
C1s, O1s, and N1s XPS spectra of the samples of microbial-derived OM-mineral composites.

TABLE 2 Assignments and quantification of XPS spectral bands for surfaces of microbial-derived OM-mineral composites.

Name	Total C (%)	Total N (%)	Total O (%)	C1s (%)		N1s (%)			O1s (%)		(N+O)/C
				C-C	C-O	C=O	399.9	402	C-O	Fe-O	
GF	6.56	0.65	23.37	63.24	26.10	10.66	71.21	28.79	72.60	27.40	2.76
PF	20.23	1.19	27.25	57.14	30.72	12.14	85.86	14.14	72.69	27.31	1.06
BF	8.29	0.50	24.78	57.74	32.56	9.69	54.66	45.34	70.21	29.79	2.29
FQ	9.68	0.31	22.40	75.85	15.79	8.36	51.56	48.44	83.63	16.37	1.76
GM	6.03	0.66	21.78	52.61	32.08	15.31	25.14	74.86	100	—	2.80
PM	5.14	0.31	21.20	51.58	37.84	10.58	42.54	57.46	100	—	3.15
BM	9.25	0.33	22.53	61.31	29.03	9.66	35.65	64.35	100	—	1.86
MQ	4.35	0.29	23.82	63.69	27.93	8.38	44.99	55.01	100	—	4.16

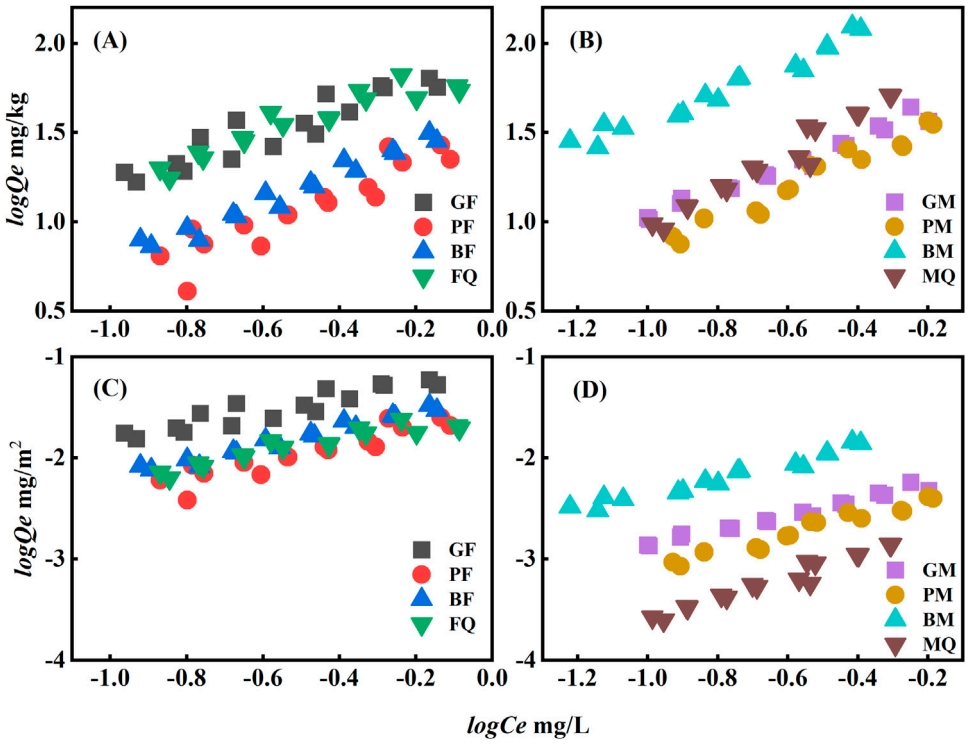

FIGURE 3
Sorption isotherms of PHE on eight adsorbents (solid phase concentration in mg/kg in **(A, B)**, and sorption isotherms normalized by SSA solid phase concentration in mg/m^2 in **(C, D)**.

OM-hematite complex contained not only oxygen atoms in the C-O form but also in the Fe-O form and both complexes had a lower nitrogen content.

3.2 Sorption comparison of PHE and OFL on microbial-derived OM-mineral composites

The sorption of PHE and OFL onto the microbial-derived OM-mineral composites was fitted using Henry's linear, Freundlich's, and Langmuir's equations. The fitting results are listed in Supplementary Table S2. By comparing the various parameters of the three models, the Freundlich model was found to be more appropriate for explaining the sorption of PHE and OFL. The n values for PHE and OFL were in the ranges of 0.639–1.081 and 0.150–2.035, respectively (Supplementary Table S2). The n values for PHE and OFL adsorbed by GF, PF, BF, and FQ were less than 1.0, whereas those for OFL adsorbed by GM, PM, BM, and M were greater than one. According to the relationship between the shape of the sorption isotherm and the n value (Calvet, 1989), the sorption

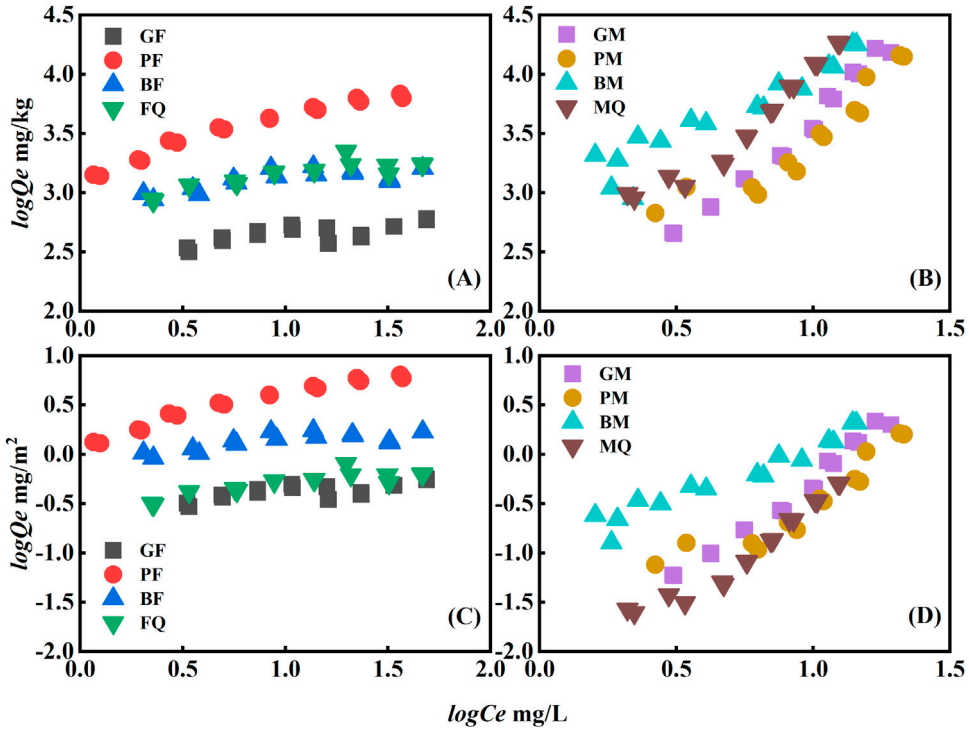

FIGURE 4
Sorption isotherms of OFL on eight adsorbents (solid phase concentration in mg/kg in **(A, B)** and sorption isotherms normalized by SSA solid phase concentration in mg/m^2 in **(C, D)**).

isotherms of PHE and OFL by microbial-derived OM-hematite composites had an "L" shape (n < 1.0). In the initial sorption period, the microbial-derived OM-hematite composites had a greater affinity for PHE and OFL, with a decrease in sorption as their concentration increased. The sorption isotherms of OFL by GM, PM, and BM were all of "S" type (n > 1.0). Conversely, the sorption of PHE was of the "L" type (n < 1), indicating that the microbial-derived OM-montmorillonite composites had a relatively weaker affinity for OFL. At low OFL concentrations, the water molecules competed with the composites for sorption. Additional research has shown that when the concentration of OFL is low, water molecules would compete for sorption sites, resulting in decreased sorption (Sukul et al., 2008).

The sorption of PHE by FQ and GF was greater than that of BF and PF (Figure 3A) and the nonlinearity was stronger than that of the other adsorbents, with the *n* value deviating the most from 1.0 (Supplementary Table S2). Compared to BF and PF, FQ and GF had greater SSA (Table 1). Thus, the sorption of PHE by microbial-derived OM-hematite composites may be related to the SSA (Kleineidam et al., 2002; Zhang et al., 2013). The carbon content of the microbial-derived OM bound to minerals increased, whereas their SSA decreased (Table 1). This may be due to the organic matter covering the mineral surface, which reduces its active sites and thus reduces the sorption power of PHE. Upon normalization of the SSA (Figure 3C), the sorption isotherms of PHE by the microbial-derived OM-hematite composites appeared to be essentially identical. This further supports the notion that SSA is a crucial factor. In addition, although the oxygen contents of GF, PF, BF, and FQ were similar (Table 1), the oxygen content on the surface of PF and BF was higher than that of GF and FQ according to XPS analysis (Table 2), and the oxygen restricted the sorption of nonpolar compounds, especially on the surface, which is consistent with previous studies (Oh et al., 2008; Cheng et al., 2018). Thus, the sorption of PHE onto the composites was mainly controlled by hydrophobic interactions.

In the microbial-derived OM-montmorillonite composites, the sorption of PHE by BM was significantly higher than that of the others (Figure 3B). After standardizing the SSA (Figure 3D), BM still showed good OFL sorption, whereas MQ had the lowest OFL sorption, which was no longer close to that of GM and PM. Moreover, MQ had the largest SSA, the large SSA is most likely the key to the sorption of OFL by MQ. Compared with GM and PM, BM had the highest aromatic content (C/H ratio of 1.10), whereas the SSA were similar (7.649–8.856 m^2/g). This suggests that the aromatics of the organic matter in the BM played an important role in the sorption of PHE. Additionally, the olefinic C=C and aromatic C=C structure of BM could form π-π conjugation, which enhanced the sorption of PHE. Similarly, XPS showed that BM, with a higher surface carbon content, had a higher sorption of PHE than PM and MQ. The above results confirmed that the sorption of PHE by microbial-derived OM-montmorillonite composites was affected by the carbon content.

The sorption of OFL by PF and BF was higher than that of FQ and GF (Figure 4A). The sorption mechanism of the microbial-derived OM-hematite composites for OFL was investigated using

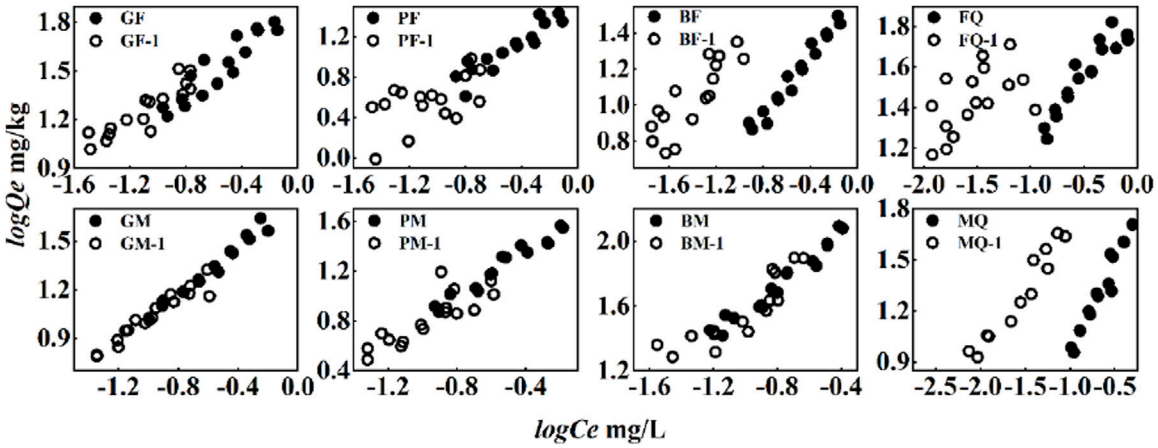

FIGURE 5
PHE sorption and desorption isotherms on eight adsorbents. The symbols (●, ○) represent the sorption equilibrium and the first desorption, respectively.

SSA standardization (Figure 4C) and the sorption of OFL by FQ decreased significantly. The sorption of OFL by FQ was greatly affected by the SSA, whereas a large difference was observed in the sorption of OFL by PF, BF, and GF, indicating the presence of other factors controlling its sorption by the composites in addition to the SSA. To investigate the sorption mechanisms of OFL by the microbial-derived OM-hematite composites, zeta potential measurements were performed, and all eight adsorbents were electronegative (Supplementary Table S3). The pH ranged from 8.31 to 9.66 after the sorption equilibrium was reached and OFL was negatively charged within this pH range (Supplementary Table S1, pKa = 8.28). Therefore, no electrostatic effect was observed on the sorption of OFL on the microbial-derived OM-hematite composites. Combined with the results of surface elemental content determined by XPS, the sorption of OFL was found to be positively correlated with the surface carbon content, with the highest carbon content for PF and the lowest for GF, corresponding to the highest and lowest maximum sorption capacity for OFL, respectively. Furthermore, the carboxyl group (-COOH) of OFL can bind to -OH on the surface of microbial-derived OM-hematite composites through esterification (Zhang and Huang, 2006; Qu et al., 2008), whereas the F, N, and O contained in OFL can form hydrogen bonds with -OH and enhance the sorption of OFL.

The order of sorption of OFL by the microbial-derived OM-montmorillonite composites was BM ≥ MQ > GM ≈ PM (Figure 4B). With the loading of microbial-derived OM on montmorillonite, the SSA of montmorillonite decreased, and its surface properties changed (Table 1). The sorption of OFL by the microbial-derived OM-montmorillonite composites showed the same trend when normalized by the SSA (Figure 4D). Similarly, the zeta potential of the microbial-derived OM-montmorillonite composites was negatively charged, and electrostatic interactions did not promote their sorption to OFL. Consistent with the microbial-derived OM-hematite composites, the sorption of OFL by the microbial-derived OM-montmorillonite composites was correlated with the carbon content of their surfaces.

3.3 Desorption characteristics of PHE and OFL

The desorption of PHE by the composites was not linear and desorption hysteresis was observed (Figure 5), indicating that the sorption of PHE and OFL on the composites was strong and stable. Microbial-derived OM cultured with glycine and glucose (G- and P-, respectively) showed stronger desorption of PHE and OFL. Although the sorption of PHE by GF was the strongest, the sorption was observed to be unstable (Figure 5). According to the sorption and desorption isotherms of OFL by the eight adsorbents, almost no desorption was observed for OFL and the sorption of OFL was very stable (Figure 6).

The degree of desorption was measured based on the desorption-release rate (*RR*). The *RR* of PHE adsorbed by the composites was positively correlated with its concentration in the solid phase (Figures 7A, B). As the concentration of PHE increased, the *RR* increased, and desorption was relatively easy. Conversely, the sorption of OFL by the composites was stable with a low *RR* and the *RR* was almost zero for both low and high concentrations of OFL (Figures 7C, D). The low *RR* may be related to the nonlinear sorption of OFL, which is more difficult to release from specific sorption sites, such as hydrogen bonds (Boyd et al., 2001; Zhang et al., 2012), resulting in a strong desorption hysteresis phenomenon.

The sorption stabilities of the composites cultured with substrate-C were different (Figure 7) and the desorption *RR* of PHE by the composites formed with 2,6-dimethoxyphenol (B-) as substrate-C was the lowest, indicating that the sorption of PHE by the composites cultured with the more complex substrate-C was more stable. The sorption characteristics and mechanisms according to the above results showed that the sorption of PHE was mainly achieved by hydrophobic interaction and highly aromatic components of microbial-derived OM could form π-π conjugation with PHE. PHE adsorbed via hydrophobic partitioning is susceptible to desorption because of environmental changes. The BM was highly aromatic and had a high sorption capacity. The PHE

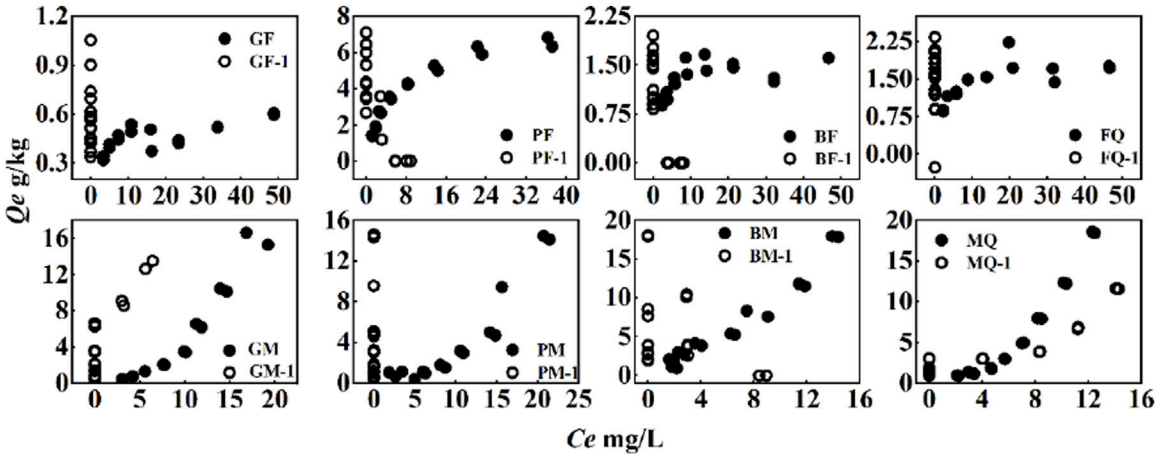

FIGURE 6
OFL sorption and desorption isotherms on eight adsorbents. The symbols (●, ○) represent the sorption equilibrium and the first desorption, respectively.

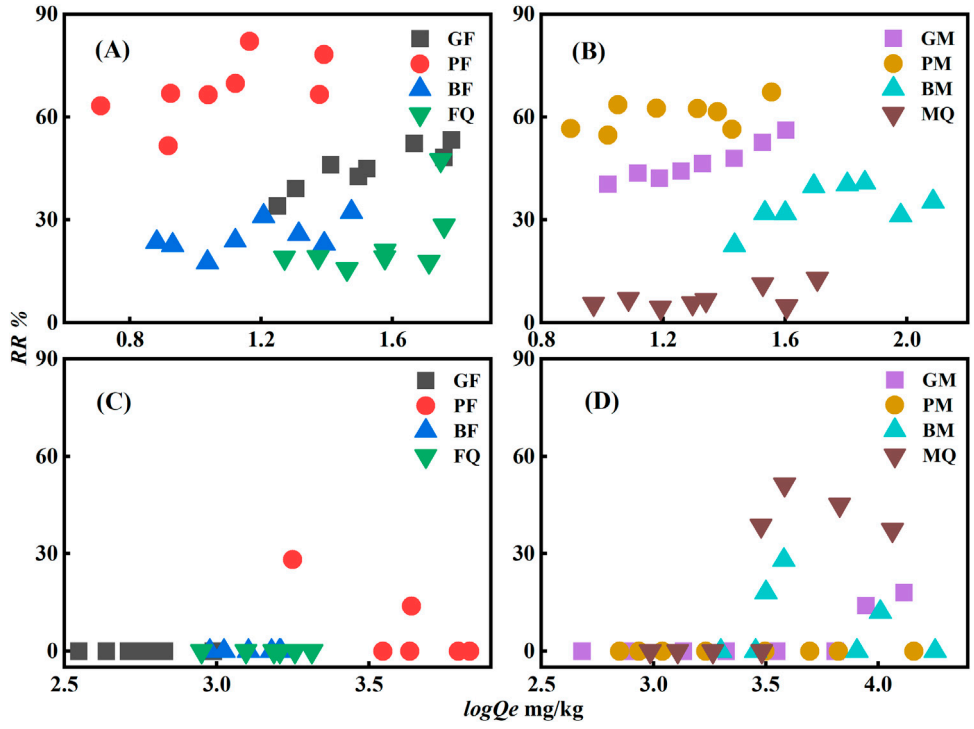

FIGURE 7
RR-log *Qe* relationship of eight adsorbents for PHE and OFL (**(A, B)** are PHE, and **(C, D)** are OFL).

adsorbed by π-π conjugation was relatively stable and desorption less. The aromaticity of the composites played an important role in the stable sorption of PHE and controlled its migration and transformation in soil. Compared with the sorption of PHE, the sorption of OFL was controlled by hydrogen bonding and π-π conjugation, thus the sorption of OFL by the eight adsorbents was more stable and difficult to be desorbed.

4 Conclusion

The microbial-derived OM -montmorillonite composites were generally more hydrophobic than microbial-derived OM-hematite composites. In addition, the higher carbon content of the montmorillonite composites, indicated a greater accumulation of microbial-derived OM formed on montmorillonite. The sorption of OFL was more dependent on the surface sites of the hematite. The

sorption of PHE on microbial-derived OM-montmorillonite composites was not only dependent on the SSA but also on the components of the microbial-derived OM formed on the minerals, especially the aromatic components. The sorption trend of OFL on the microbial-derived OM-hematite composites was opposite to that of PHE. Hydrophobic interaction and π-π conjugation dominated the sorption of PHE on the composites. The sorption of OFL was controlled by a combination of hydrogen bonding and π-π conjugation. BM had the highest aromaticity and the highest sorption through the strong π-π conjugation. The sorption of OFL by the composites was higher and more stable than that of PHE and the OFL sorbed on the composites was relatively stable, as reflected by the stronger desorption hysteresis. Therefore, organic contaminants, especially ionic organic contaminants, can be immobilized in soil through their interaction with microbial-derived OM, thereby reducing the ecological risk of organic contaminants.

Data availability statement

The raw data supporting the conclusions of this article will be made available by the authors, without undue reservation.

Author contributions

FL: Conceptualization, Formal Analysis, Investigation, Methodology, Writing–original draft, Writing–review and editing. QY: Data curation, Formal Analysis, Methodology, Writing–original draft. ZL: Data curation, Formal Analysis, Methodology, Writing–original draft. ZT: Formal Analysis, Software, Visualization, Writing–original draft. YL: Methodology, Writing–review and editing. SW: Methodology, Validation, Writing–review and editing. JG: Writing–review and editing. HP: Writing–review and editing. LW: Data curation, Methodology, Writing–review and editing.

Funding

The author(s) declare that financial support was received for the research, authorship, and/or publication of this article. This study was supported by the Yunnan Major Scientific and Technological Projects (grant NO. 202202AG050019), the National Natural Science Foundation of China (grant NO. 41907300, 42167030, 42267028), the Yunnan Science and Technology Planning Project (grant No. 202303AC100010), Yunnan Fundamental Research Projects (grant NO. 202101BE070001-063).

Conflict of interest

The authors declare that the research was conducted in the absence of any commercial or financial relationships that could be construed as a potential conflict of interest.

Publisher's note

All claims expressed in this article are solely those of the authors and do not necessarily represent those of their affiliated organizations, or those of the publisher, the editors and the reviewers. Any product that may be evaluated in this article, or claim that may be made by its manufacturer, is not guaranteed or endorsed by the publisher.

Supplementary material

The Supplementary Material for this article can be found online at: https://www.frontiersin.org/articles/10.3389/fenvs.2024.1485328/full#supplementary-material

References

Abollino, O., Aceto, M., Malandrino, M., Sarzanini, C., and Mentasti, E. (2003). Adsorption of heavy metals on Na-montmorillonite. Effect of pH and organic substances. *Water Res.* 37, 1619–1627. doi:10.1016/S0043-1354(02)00524-9

Ahmed, M. B., Zhou, J. L., Ngo, H. H., Johir, M. A. H., Sun, L., Asadullah, M., et al. (2018). Sorption of hydrophobic organic contaminants on functionalized biochar: protagonist role of π-π electron-donor-acceptor interactions and hydrogen bonds. *J. Hazard. Mater.* 360, 270–278. doi:10.1016/j.jhazmat.2018.08.005

Angers, D. A., and Giroux, M. (1996). Recently deposited organic matter in soil water-stable aggregates. *Soil Sci. Soc. Am. J.* 60, 1547–1551. doi:10.2136/sssaj1996.03615995006000050037x

Bolyard, S. C., Reinhart, D. R., and Richardson, D. (2019). Conventional and fourier transform infrared characterization of waste and leachate during municipal solid waste stabilization. *Chemosphere* 227, 34–42. doi:10.1016/j.chemosphere.2019.04.035

Boyd, S. A., Sheng, G., Teppen, B. J., and Johnston, C. T. (2001). Mechanisms for the adsorption of substituted nitrobenzenes by smectite clays. *Environ. Sci. Technol.* 35, 4227–4234. doi:10.1021/es010663w

Buckeridge, K. M., La Rosa, A. F., Mason, K. E., Whitaker, J., McNamara, N. P., Grant, H. K., et al. (2020). Sticky dead microbes: rapid abiotic retention of microbial necromass in soil. *Soil Biol. biochem.* 149, 107929. doi:10.1016/j.soilbio.2020.107929

Cai, Y., Ma, T., Wang, Y. Y., Jia, J., Jia, Y. F., Liang, C., et al. (2021). Assessing the accumulation efficiency of various microbial carbon components in soils of different minerals. *Geoderma* 407, 115562. doi:10.1016/j.geoderma.2021.115562

Calvet, R. (1989). Adsorption of organic chemicals in soils. *Environ. Health Persp.* 83, 145–177. doi:10.1289/ehp.8983145

Chen, H., Li, Q., Wang, M., Ji, D., and Tan, W. (2020). XPS and two-dimensional FTIR correlation analysis on the binding characteristics of humic acid onto kaolinite surface. *Sci. Total Environ.* 724, 138154. doi:10.1016/j.scitotenv.2020.138154

Chen, R., Cai, B., Liu, R., Xu, W., Jin, X., Yu, L., et al. (2024). Synergistic and antagonistic adsorption mechanisms of copper(II) and cefazolin onto bio-based chitosan/humic composite: a combined experimental and theoretical study. *J. Environ. Chem. Eng.* 12, 113061. doi:10.1016/j.jece.2024.113061

Chen, Y. Q., Wang, M. L., Zhou, X. W., Fu, H. Y., Qu, X. L., and Zhu, D. Q. (2020). Sorption fractionation of bacterial extracellular polymeric substances (EPS) on mineral surfaces and associated effects on phenanthrene sorption to EPS-mineral complexes. *Chemosphere* 263, 128264. doi:10.1016/j.chemosphere.2020.128264

Cheng, Z., Zhang, X., Kennes, C., Chen, J., Chen, D., Ye, J., et al. (2018). Differences of cell surface characteristics between the bacterium Pseudomonas veronii and fungus Ophiostoma stenoceras and their different adsorption properties to hydrophobic organic compounds. *Sci. Total Environ.* 650, 2095–2106. doi:10.1016/j.scitotenv.2018.09.337

Chi, J., Zhang, W., Wang, L., and Putnis, C. V. (2019). Direct observations of the occlusion of soil organic matter within calcite. *Environ. Sci. Technol.* 53, 8097–8104. doi:10.1021/acs.est.8b06807

Chu, G., Zhao, J., Liu, Y., Lang, D., Wu, M., Pan, B., et al. (2019). The relative importance of different carbon structures in biochars to carbamazepine and bisphenol A sorption. *J. Hazard. Mater.* 373, 106–114. doi:10.1016/j.jhazmat.2019.03.078

Das, S., Paul, S. R., and Debnath, A. (2024). Enhanced performance of Lagerstroemia speciosa seed biochar and polypyrrole composite for the sequestration of emerging contaminant from wastewater sample: case study of ofloxacin drug. *J. Water Process Eng.* 64, 105699. doi:10.1016/j.jwpe.2024.105699

Disi, Z. A. A., Mohamed, D. O., Al-Ghouti, M. A., and Zouari, N. (2023). Insights into the interaction between mineral formation and heavy metals immobilization, mediated by virgibacillus exopolymeric substances. *Environ. Technol. Inno* 33, 103477. doi:10.1016/j.eti.2023.103477

Duchaufour, P. (1976). Dynamics of organic matter in soils of temperate regions: its action on pedogenesis. *Geoderma* 15, 31–40. doi:10.1016/0016-7061(76)90068-9

Feng, M., Yan, L., Zhang, X., Sun, P., Yang, S., Wang, L., et al. (2015). Fast removal of the antibiotic flumequine from aqueous solution by ozonation: influencing factors, reaction pathways, and toxicity evaluation. *Sci. Total Environ.* 541, 167–175. doi:10.1016/j.scitotenv.2015.09.048

Feng, W., Liu, H., Yu, Y. Y., Jiao, S. H., Biney, B. W., Ibrahim, U. K., et al. (2021). Study on the formation of olefinic-bond-containing asphaltenes during thermal cracking of vacuum residue. *Fuel* 304, 121365. doi:10.1016/j.fuel.2021.121365

Gao, H., Ma, J., Xu, L., and Jia, L. (2014). Hydroxypropyl-β-cyclodextrin extractability and bioavailability of phenanthrene in humin and humic acid fractions from different soils and sediments. *Environ. Sci. Pollut. R.* 21, 8620–8630. doi:10.1007/s11356-014-2701-6

Gauthier, M. A., Stangel, I., Ellis, T. H., and Zhu, X. X. (2005). A new method for quantifying the intensity of the C=C band of dimethacrylate dental monomers in their FTIR and Raman spectra. *Biomaterials* 26, 6440–6448. doi:10.1016/j.biomaterials.2005.04.039

Goldman, R., Enewold, L., Pellizzari, E., Beach, J. B., Bowman, E. D., Krishnan, S. S., et al. (2001). Smoking increases carcinogenic polycyclic aromatic hydrocarbons in human lung tissue. *Cancer Res.* 61, 6367–6371.

He, Y., Zeng, F. F., Lian, Z. H., Xu, J. M., and Brookes, P. C. (2015). Natural soil mineral nanoparticles are novel sorbents for pentachlorophenol and phenanthrene removal. *Environ. Pollut.* 205, 43–51. doi:10.1016/j.envpol.2015.05.021

Hu, J., Du, M., Chen, J., Tie, L., Zhou, S., Buckeridge, K. M., et al. (2023). Microbial necromass under global change and implications for soil organic matter. *Glob. Change Biol.* 29, 3503–3515. doi:10.1111/gcb.16676

Kaiser, K., and Zech, W. (1997). Competitive sorption of dissolved organic matter fractions to soils and related mineral phases. *Soil Sci. Soc. Am. J.* 61, 64–69. doi:10.2136/sssaj1997.03615995006100010011x

Kallenbach, C. M., Frey, S. D., and Grandy, A. S. (2016). Direct evidence for microbial-derived soil organic matter formation and its ecophysiological controls. *Nat. Commun.* 7, 13630. doi:10.1038/ncomms13630

Kallenbach, C. M., Frey, S. D., and Grandy, A. S. (2018). Author Correction: direct evidence for microbial-derived soil organic matter formation and its ecophysiological controls. *Nat. Commun.* 9, 3929. doi:10.1038/s41467-018-06427-3

Kleineidam, S., Schüth, C., and Grathwohl, P. (2002). Solubility-normalized combined adsorption-partitioning sorption isotherms for organic pollutants. *Environ. Sci. Technol.* 36, 4689–4697. doi:10.1021/es010293b

Lee, B. M., Shin, H. S., and Hur, J. (2013). Comparison of the characteristics of extracellular polymeric substances for two different extraction methods and sludge formation conditions. *Chemosphere* 90, 237–244. doi:10.1016/j.chemosphere.2012.06.060

Li, F. F., Pan, B., Liang, N., Chang, Z. F., Zhou, Y. W., Wang, L., et al. (2017). Reactive mineral removal relative to soil organic matter heterogeneity and implications for organic contaminant sorption. *Environ. Pollut.* 227, 49–56. doi:10.1016/j.envpol.2017.04.047

Li, R. L., Ren, L. F., Yu, S. J., Liu, H. Q., Sun, X., and Qiang, T. T. (2024). Construction of fulvic acid-based chrome-free tanning agent with on-demand regulation and wastewater recycling: a novel tanning-dyeing integrated strategy. *Chem. Eng. J.* 482, 148892. doi:10.1016/j.cej.2024.148892

Li, Y., Bi, E., and Chen, H. (2019). Effects of dissolved humic acid on fluoroquinolones sorption and retention to kaolinite. *Ecotox. Environ. Safe.* 178, 43–50. doi:10.1016/j.ecoenv.2019.04.002

Liang, C., Amelung, W., Lehmann, J., and Kästner, M. (2019). Quantitative assessment of microbial necromass contribution to soil organic matter. *Glob. Change Biol.* 25, 3578–3590. doi:10.1111/gcb.14781

Liang, C., Kästner, M., and Joergensen, R. G. (2020). Microbial necromass on the rise: the growing focus on its role in soil organic matter development. *Soil Biol. biochem.* 150, 108000. doi:10.1016/j.soilbio.2020.108000

Liang, C., and Zhu, X. (2021). The soil microbial carbon pump as a new concept for terrestrial carbon sequestration. *Sci. China Earth Sci.* 64, 545–558. doi:10.1007/s11430-020-9705-9

Liang, N., Zhang, D., Wei, C., Li, H., Ghosh, S., Cao, Y., et al. (2015). Comparative adsorption of phenanthrene, bisphenol A, and sulfamethoxazole on humic acid-iron oxide nanoparticle complexes. *Environ. Eng. Sci.* 32, 703–712. doi:10.1089/ees.2015.0025

Luo, L., Lv, J. T., Chen, Z. E., Huang, R. X., and Zhang, S. Z. (2017). Insights into the attenuated sorption of organic compounds on black carbon aged in soil. *Environ. Pollut.* 231, 1469–1476. doi:10.1016/j.envpol.2017.09.010

Mikutta, R., Mikutta, C., Kalbitz, K., Scheel, T., Kaiser, K., and Jahn, R. (2007). Biodegradation of forest floor organic matter bound to minerals via different binding mechanisms. *Geochim. Cosmochim. Ac.* 71, 2569–2590. doi:10.1016/j.gca.2007.03.002

Mohan, A. J., Sekhar, V. C., Bhaskar, T., and Nampoothiri, K. M. (2016). Microbial assisted high impact polystyrene (HIPS) degradation. *Bioresour. Technol.* 213, 204–207. doi:10.1016/j.biortech.2016.03.021

Na, P. T. L., Tuyen, N. D. K., and Dang, B. T. (2024). Sorption of four antibiotics onto pristine biochar derived from macadamia nutshell. *Bioresour. Technol.* 394, 130281. doi:10.1016/j.biortech.2023.130281

Oh, G. Y., Ju, Y. W., Kim, M. Y., Jung, H. R., Kim, H. J., and Lee, W. J. (2008). Adsorption of toluene on carbon nanofibers prepared by electrospinning. *Sci. Total Environ.* 393, 341–347. doi:10.1016/j.scitotenv.2008.01.005

Olayo, M. G., Alvarado, E. J., González-Torres, M., Gómez, L. M., and Cruz, G. J. (2023). Quantifying amines in polymers by XPS. *Polym. Bull.* 81, 2319–2328. doi:10.1007/s00289-023-04829-y

Pakova, V., Hilscherova, K., Feldmannova, M., and Blaha, L. (2006). Toxic effects and oxidative stress in higher plants exposed to polycyclic aromatic hydrocarbons and their N-heterocyclic derivatives. *Environ. Toxicol. Chem.* 25, 3238–3245. doi:10.1897/06-162R.1

Pan, B., Huang, P., Wu, M., Wang, Z. Y., Wang, P., Jiao, X. C., et al. (2011). Physicochemical and sorption properties of thermally-treated sediments with high organic matter content. *Bioresour. Technol.* 103, 367–373. doi:10.1016/j.biortech.2011.09.054

Pan, B., Xing, B. S., Liu, W. X., Tao, S., Lin, X. M., Zhang, X. M., et al. (2005). Distribution of sorbed phenanthrene and pyrene in different humic fractions of soils and importance of humin. *Environ. Pollut.* 143, 24–33. doi:10.1016/j.envpol.2005.11.009

Papageorgiou, S. K., Kouvelos, E. P., Favvas, E. P., Sapalidis, A. A., Romanos, G. E., and Katsaros, F. K. (2010). Metal-carboxylate interactions in metal-alginate complexes studied with FTIR spectroscopy. *Carbohyd. Res.* 354, 469–473. doi:10.1016/j.carres.2009.12.010

Peng, H. B., Pan, B., Wu, M., Liu, Y., Zhang, D., and Xing, B. S. (2012). Adsorption of ofloxacin and norfloxacin on carbon nanotubes: hydrophobicity- and structure-controlled process. *J. Hazard. Mater.* 233, 89–96. doi:10.1016/j.jhazmat.2012.06.058

Qu, X. L., Xiao, L., and Zhu, D. Q. (2008). Site-specific adsorption of 1,3-dinitrobenzene to bacterial surfaces: a mechanism of n-pi electron-donor-acceptor interactions. *J. Environ. Qual.* 37, 824–829. doi:10.2134/jeq2007.0236

Safari, S., von Gunten, K., Alam, M. S., Hubmann, M., Blewett, T. A., Chi, Z., et al. (2019). Biochar colloids and their use in contaminants removal. *Biochar* 1, 151–162. doi:10.1007/s42773-019-00014-5

Shen, Y., Li, J. F., He, F., Zhu, J. H., Han, Q., Zhan, X. H., et al. (2019). Phenanthrene-triggered tricarboxylic acid cycle response in wheat leaf. *Sci. Total Environ.* 665, 107–112. doi:10.1016/j.scitotenv.2019.02.119

Shukla, N., Svedberg, E. B., and Ell, J. (2007). Surfactant isomerization and dehydrogenation on FePt nanoparticles. *Colloid Surf. A* 301, 113–116. doi:10.1016/j.colsurfa.2006.12.031

Su, X. Y., Zhang, R. J., Cao, H., Mu, D. C., Wang, L. Q., Song, C. H., et al. (2024). Adsorption of humic acid from different organic solid waste compost to phenanthrene, is fluorescence excitation or quenching? *Environ. Pollut.* 347, 123712. doi:10.1016/j.envpol.2024.123712

Sukul, P., Lamshöft, M., Zühlke, S., and Spiteller, M. (2008). Sorption and desorption of sulfadiazine in soil and soil-manure systems. *Chemosphere* 73, 1344–1350. doi:10.1016/j.chemosphere.2008.06.066

Tabak, A., Sevimli, K., Kaya, M., and Çağlar, B. (2019). Preparation and characterization of a novel activated carbon component via chemical activation of tea woody stem. *J. Therm. Anal. Calorim.* 138, 3885–3895. doi:10.1007/s10973-019-08387-2

Wang, L. T., Hua, X. Y., Zhang, L. W., Song, N., Dong, D. M., and Guo, Z. Y. (2019). Influence of organic carbon fractions of freshwater biofilms on the sorption for phenanthrene and ofloxacin: the important role of aliphatic carbons. *Sci. Total Environ.* 685, 818–826. doi:10.1016/j.scitotenv.2019.06.203

Wen, B., Zhang, J. J., Zhang, S. Z., Shan, X. Q., Khan, S. U., and Xing, B. S. (2007). Phenanthrene sorption to soil humic acid and different humin fractions. *Environ. Sci. Technol.* 41, 3165–3171. doi:10.1021/es062262s

Wu, M., Pan, B., Zhang, D., Xiao, D., Li, H., Wang, C., et al. (2012). The sorption of organic contaminants on biochars derived from sediments with high organic carbon content. *Chemosphere* 90, 782–788. doi:10.1016/j.chemosphere.2012.09.075

Xia, X. L., Han, X., and Zhai, Y. Z. (2024). Activation of iron oxide minerals in an aquifer by humic acid to promote adsorption of organic molecules. *J. Environ. Manage.* 356, 120543. doi:10.1016/j.jenvman.2024.120543

Xiao, K. Q., Zhao, Y., Liang, C., Zhao, M., Moore, O. W., Otero-Fariña, A., et al. (2023). Introducing the soil mineral carbon pump. *Nat. Rev. Earth Env.* 4, 135–136. doi:10.1038/s43017-023-00396-y

Xing, J., Dong, W., Liang, N., Huang, Y., Wu, M., Zhang, L., et al. (2023). Sorption of organic contaminants by biochars with multiple porous structures: experiments and molecular dynamics simulations mediated by three-dimensional models. *J. Hazard. Mater.* 458, 131953. doi:10.1016/j.jhazmat.2023.131953

Xu, Q. Y., Han, B., Wang, H. D., Wang, Q. D., Zhang, W. J., and Wang, D. S. (2020). Effect of extracellular polymer substances on the tetracycline removal during coagulation process. *Bioresour. Technol.* 309, 123316. doi:10.1016/j.biortech.2020.123316

Yan, J. C., Lei, Z. P., Li, Z. K., Wang, Z. C., Ren, S. B., Kang, S. G., et al. (2020). Molecular structure characterization of low-medium rank coals via XRD, solid state 13C NMR and FTIR spectroscopy. *Fuel* 268, 117038. doi:10.1016/j.fuel.2020.117038

Yang, L. J., Chen, Z., Zhang, Y., Lu, F. P., Liu, Y. H., Cao, M. F., et al. (2023). Hyperproduction of extracellular polymeric substance in Pseudomonas fluorescens for efficient chromium (VI) absorption. *Bioresour. Bioprocess.* 10, 17. doi:10.1186/s40643-023-00638-3

Zhang, D., Pan, B., Wu, M., Zhang, H., Peng, H., Ning, P., et al. (2012). Cosorption of organic chemicals with different properties: their shared and different sorption sites. *Environ. Pollut.* 160, 178–184. doi:10.1016/j.envpol.2011.08.053

Zhang, H., and Huang, C. H. (2006). Adsorption and oxidation of fluoroquinolone antibacterial agents and structurally related amines with goethite. *Chemosphere* 66, 1502–1512. doi:10.1016/j.chemosphere.2006.08.024

Zhang, L., Liu, F., and Chen, L. (2017). Sorption specificity and desorption hysteresis of gibberellic acid on ferrihydrite compared to goethite, hematite, montmorillonite, and kaolinite. *Environ. Sci. Pollut. R.* 24, 19068–19075. doi:10.1007/s11356-017-9445-z

Zhang, P., Sun, H. W., Yu, L., and Sun, T. H. (2013). Adsorption and catalytic hydrolysis of carbaryl and atrazine on pig manure-derived biochars: impact of structural properties of biochars. *J. Hazard. Mater.* 244, 217–224. doi:10.1016/j.jhazmat.2012.11.046

Zhang, Q. Q., Ying, G. G., Pan, C. G., Liu, Y. S., and Zhao, J. L. (2015). Comprehensive evaluation of antibiotics emission and fate in the river basins of China: source analysis, multimedia modeling, and linkage to bacterial resistance. *Environ. Sci. Technol.* 49, 6772–6782. doi:10.1021/acs.est.5b00729

Zhao, C. H., Hu, L. L., Zhang, C. A., Wang, S. S., Wang, X. Z., and Huo, Z. Y. (2021). Preparation of biochar-interpenetrated iron-alginate hydrogel as a pH-independent sorbent for removal of Cr(VI) and Pb(II). *Environ. Pollut.* 287, 117303. doi:10.1016/j.envpol.2021.117303

Zhu, M. P., Zhou, K. B., Sun, X. D., Zhao, Z. X., Tong, Z. F., and Zhao, Z. X. (2017). Hydrophobic N-doped porous biocarbon from dopamine for high selective adsorption of p-Xylene under humid conditions. *Chem. Eng. J.* 317, 660–672. doi:10.1016/j.cej.2017.02.114

Zhu, X., Jackson, R. D., DeLucia, E. H., Tiedje, J. M., and Liang, C. (2020). The soil microbial carbon pump: from conceptual insights to empirical assessments. *Glob. Change Biol.* 26, 6032–6039. doi:10.1111/gcb.15319